

The effect of the stochasticity of photoionization on 3D streamer simulations

B. Bagheri¹, J. Teunissen^{1,2}

¹Centrum Wiskunde & Informatica, Amsterdam, The Netherlands

²Centre for Mathematical Plasma-Astrophysics, KU Leuven, Belgium

E-mail: b.bagheri@cwi.nl

28 January 2022

Abstract. Positive streamer discharges require a source of free electrons ahead of them for their growth. In air, these electrons are typically provided by photoionization. Here we investigate how stochastic fluctuations due to the discreteness of ionizing photons affect positive streamers in air. We simulate positive streamers between two planar electrodes with a 3D plasma fluid model, using both a stochastic and a continuum method for photoionization. With stochastic photoionization, fluctuations are visible in the streamer's direction, maximal electric field, velocity, and electron density. The streamers do not branch, and we find good agreement between the averaged stochastic results and the results with continuum photoionization. The streamers stay roughly axisymmetric, and we show that results obtained with an axisymmetric model indeed agree well with the 3D results. However, we find that positive streamers are sensitive to the amount of photoionization. When the amount of photoionization is doubled, there is even better agreement between the stochastic and continuum results, but with half the amount of photoionization, stochastic fluctuations become more important and streamer branching starts to occur.

1. Introduction

Streamers [1–3] are rapidly growing electric discharges with an elongated shape. They can appear when the electric field in a nonconducting medium exceeds the breakdown threshold. Streamer channels are surrounded by a space charge layer that enhances the electric field at their tips, where electron impact ionization causes them to grow. Due to their electric field enhancement, streamers can propagate into regions where the background field is below the breakdown threshold. Streamers typically occur in gases [4], although they can also form in liquids [5].

Streamers are the precursors to lightning leaders and sparks, and they can be observed directly as sprites [6] above thunderstorms. In technology, streamers are used in diverse applications [7, 8], for example for the production of chemical radicals [9], in ignition and combustion [10] and plasma catalysis [11]. Because streamer channels are weakly ionized, they typically do not significantly increase the gas temperature.

Streamers can be of positive or negative polarity. Positive streamers propagate typically in the direction of the electric field. Negative streamers propagate in the opposite direction. In this paper we focus on positive streamers, which in air form more easily than negative ones [12]. Because positive streamers propagate against the electron drift velocity, they require a source of free electrons ahead of them. When these electrons enter the high-field region around a positive streamer head they rapidly multiply due to electron-impact ionization, which causes the streamer channel to extend. The propagation of positive streamers can therefore be quite sensitive to the distribution of free electrons ahead of them [13].

In air, photoionization is typically the most important source of free electrons [4, 14] ahead of positive streamers. This process occurs when a UV photon emitted by an excited nitrogen molecule ionizes an oxygen molecule. A commonly used model for photoionization is Zheleznyak’s model [15]. Recent work has suggested several refinements to Zheleznyak’s model, such as the generalization to other gas mixtures [16], the inclusion of multiple excited states and transitions [17, 18] and taking the lifetime of excited states into account [19].

Numerical solutions to Zheleznyak’s photoionization model are often computed using the so-called Helmholtz approximation, in which the absorption function of the produced photons is written in terms of an exponential expansion [20, 21]. The photoionization profile can then be computed as a density from a set of Helmholtz equations. In reality, photoionization is a stochastic process, in which the ionizing photons are discrete. Discrete photoionization events can be gen-

erated using Monte Carlo methods, as was first done in [22].

Stochastic fluctuations due to photoionization are likely to dominate over fluctuations due to e.g., the discreteness of electrons, because of the relatively low photon numbers and long absorption distances. The goal of the present paper is therefore to study how fluctuations due to photoionization affect positive streamers in atmospheric air. We investigate the role of these fluctuations using 3D plasma fluid simulations, and compare results with stochastic photoionization to results with a continuum approximation for photoionization. We also study how sensitive the evolution of positive streamers is to the amount of photoionization. Furthermore, the 3D results are compared to axisymmetric simulations performed with a model that was recently benchmarked against five other codes [23].

Comparison with earlier work: In [24], a fluid model was used to study the effect of stochastic photoionization on streamer propagation and branching in a 2D Cartesian geometry. An important difference with the present paper is that in this work we perform 3D simulations, which are required to realistically capture stochastic fluctuations. The role of stochastic electron density fluctuations for streamer branching was investigated in [25], and in [26] the effect of such fluctuations on the onset of branching for negative streamers was studied, but in overvolted gaps and without photoionization. There exist several papers about PIC (particle-in-cell) simulations of streamers including stochastic photoionization, for example [18, 22, 27], but these simulations are typically limited to short propagation lengths due to their high computational cost. Another new contribution of this paper is that we compare stochastic photoionization to the common continuum approach.

The structure of the paper is as follows. The plasma fluid model and simulation conditions are described in section 2, after which the photoionization approaches are described in section 3. In section 4 stochastic and continuum photoionization are compared using both 3D and axisymmetric simulations. Furthermore, the number of UV photons is varied to show when stochastic effects become important.

2. Discharge model and conditions

We use a plasma fluid model of the drift-diffusion-reaction type coupled to the local field approximation, as implemented in [28]. A fluid model cannot correctly capture all the physical noise in a simulation, but on the other hand, PIC simulations typically introduce too much noise, when they employ super-particles. Using a fluid model for the electron density allows us to single

out the noise due to the discreteness of the photons and the photoionization. Another advantage of fluid models is that they are computationally much cheaper than PIC codes.

In [23], our plasma fluid model [28] for streamer discharges was compared with models from five other groups. Axisymmetric simulations of positive streamers were performed. For sufficiently fine grids and small time steps, reasonably good agreement between the models was found.

The comparison study [23] included one test case with photoionization, using the Helmholtz approximation. Here we generalize that test case in two ways: First, stochastic fluctuations due to photoionization are taken into account. Second, the simulations are performed in 3D, to realistically model fluctuations and their effect on the streamer's propagation. We use the same fluid model, transport coefficients, computational domain and photoionization parameters as in [23].

2.1. Model equations

The electron density n_e and positive ion density n_i evolve in time as

$$\partial_t n_e = \nabla \cdot (n_e \mu_e \mathbf{E} + D_e \nabla n_e) + S_i + S_{ph}, \quad (1)$$

$$\partial_t n_i = S_i + S_{ph}, \quad (2)$$

in which μ_e is the (positive) electron mobility, D_e the electron diffusion coefficient, $\bar{\alpha}$ the effective ionization coefficient, \mathbf{E} the electric field, $S_i = \bar{\alpha} \mu_e |\mathbf{E}| n_e$ the ionization source term and S_{ph} the non-local photoionization source term (see section 3). Ion motion is neglected. The electric field is computed in the electrostatic approximation as

$$\begin{aligned} \mathbf{E} &= -\nabla \phi, \\ \nabla^2 \phi &= -\frac{e(n_i - n_e)}{\epsilon_0}, \end{aligned}$$

where ϕ is the electric potential, ϵ_0 the vacuum permittivity, and e the elementary charge.

We consider streamer discharges in dry air, containing 80% N₂ and 20% O₂, at $p = 1$ bar and $T = 300$ Kelvin. The local field approximation is used for the transport coefficients, so that $\bar{\alpha}$, μ_e and D_e depend on the local electric field strength. We use the same analytic transport coefficients as in [23], which were retrieved from [29, 30]. At a gas pressure of $p = 1$ bar and a gas temperature of $T = 300$ K, the coefficients can be written as

$$\mu_e = 2.3987 E^{-0.26}$$

$$D_e = 4.3628 \times 10^{-3} E^{0.22}$$

$$\bar{\alpha} = \alpha - \eta$$

$$\alpha = (1.1944 \times 10^6 + 4.3666 \times 10^{26} / E^3) e^{-2.73 \times 10^7 / E}$$

$$\eta = 340.75,$$

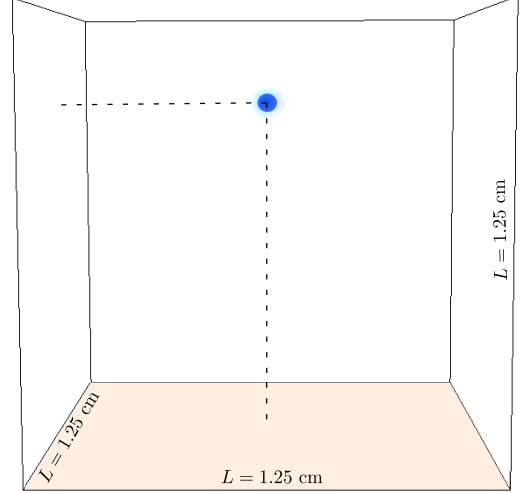


Figure 1: A 3D view of the computational domain showing the position of the initial seed from which the streamer starts. The seed has a Gaussian distribution and a maximal density of $5 \times 10^{18} \text{ m}^{-3}$ positive ions, a width of 0.4 mm, and it is located at a height of 1 cm. The top plane is at a potential of 18.75 kV and the bottom plane (colored) is grounded.

where SI units have been omitted, so that E is the electric field strength in V/m, μ_e the mobility in $\text{m}^2/(\text{Vs})$ etc. More accurate transport coefficients could be obtained by using a Boltzmann solver [31], but for the purpose of this study having highly realistic transport coefficients is not essential.

The fluid model used here is described in more detail in [28]. It is based on the Afivo framework [32], which contains geometric multigrid methods to quickly solve Poisson's equation, octree-based adaptive mesh refinement and OpenMP parallelism. The fluid equations are solved using explicit second order time stepping, and a slope-limited second order accurate spatial discretization.

2.2. Computational domain and initial conditions

The computational domain shown in fig. 1 is used for 3D simulations. It measures 1.25 cm in all three Cartesian directions. The top plane is at a potential $\phi = 18.75$ kV and the bottom plane is grounded; hence the background field is 15 kV/cm, which is about half of the breakdown field. For the potential, homogeneous Neumann boundary conditions are used on the other four sides, and for the electron density they are used on all boundaries. Instead of a needle electrode protruding from the top plate, a positive immobile seed with a Gaussian distribution is implemented. The seed is located at a height of 1 cm, and it has a maximal density of $N_0 = 5 \times 10^{18} \text{ m}^{-3}$ positive ions, and a

width of $\sigma = 0.4$ mm:

$$n_i(\mathbf{r}) = N_0 \exp \left[-\frac{(\mathbf{r} - \mathbf{r}_0)^2}{\sigma^2} \right], \quad (3)$$

where \mathbf{r}_0 indicates the location of the seed. A homogeneous background density of $n_e = n_i = 10^9 \text{ m}^{-3}$ electrons and positive ions is included. This background density facilitates the start of the discharge, after which photoionization will quickly dominate over it[‡]. For the axisymmetric simulations, we use the same computational domain as in [23].

We use the same refinement criterion as in [28], namely refine if $\alpha(1.2 \times E) \Delta x > 1.0$, where $\alpha(E)$ is the field-dependent ionization coefficient, E is the electric field strength in V/m, and Δx is the grid spacing. For the simulations in section 4 this gives an AMR grid with a minimum grid spacing of about $3 \mu\text{m}$.

3. Photoionization models

In this study, we make use of Zheleznyak's photoionization model for air [15]. Assuming that ionizing photons do not scatter and that their direction is isotropically distributed, the photoionization source term $S_{\text{ph}}(\mathbf{r})$ is given by

$$S_{\text{ph}}(\mathbf{r}) = \int d^3 r' \frac{I(\mathbf{r}') f(|\mathbf{r} - \mathbf{r}'|)}{4\pi |\mathbf{r} - \mathbf{r}'|^2}, \quad (4)$$

where $I(\mathbf{r})$ is the source of ionizing photons, $4\pi |\mathbf{r} - \mathbf{r}'|^2$ is a geometric factor, and $f(\mathbf{r})$ is the absorption function that gives the probability density of photon absorption at a distance r :

$$f(r) = \frac{\exp(-\chi_{\min} p_{O_2} r) - \exp(-\chi_{\max} p_{O_2} r)}{r \ln(\chi_{\max}/\chi_{\min})}, \quad (5)$$

where $\chi_{\max} \approx 1.5 \times 10^2 / (\text{mm bar})$, $\chi_{\min} \approx 2.6 / (\text{mm bar})$, and p_{O_2} is the partial pressure of oxygen. In Zheleznyak's model the UV photon source term $I(\mathbf{r})$ is proportional to the electron impact ionization source term S_i

$$I(\mathbf{r}) = \frac{p_q}{p + p_q} \xi S_i, \quad (6)$$

where the factor $p_q/(p + p_q)$ accounts for the collisional quenching of excited nitrogen molecules, where p is the gas pressure and we use a quenching pressure of $p_q = 40 \text{ mbar}$. The proportionality factor ξ is in principle field-dependent [15], but for simplicity we here set it to $\xi = 0.075$ (except for section 4.3, where it is varied).

As stated in the introduction, there have recently been several efforts to improve upon Zheleznyak's

[‡] As pointed out by one of the referees, a fluid model cannot accurately simulate the (stochastic) first electron avalanches originating from such a low background density. Here we have chosen to only focus on the stochastic effects of photoionization, not on the stochasticity of discharge inception.

model, for example by taking different excited states and their lifetime into account [17] or by considering different gas mixtures [16]. Since in this paper we focus on the effect of stochastic fluctuations, we use Zheleznyak's model in its standard formulation.

3.1. Continuum (Helmholtz) approach

Directly evaluating the integral in eq. (4) is computationally too expensive, in particular in 3D. In [20, 21] an approximation was proposed in which the absorption function f of eq. (5) is expanded as

$$f(r) \approx r \sum_{i=1}^N c_i e^{-\lambda_i r}, \quad (7)$$

where c_i and λ_i are fitted coefficients. When this expansion is plugged into equation (4), one obtains N Helmholtz equations that can be solved with fast elliptic solvers to obtain S_{ph} . We remark that the exponential expansion of equation (7) differs by a factor of r^2 from the form of equation (5). Therefore, the expansions can only be accurate in a certain range and not for very short absorption distances. As discussed in [20] this is often acceptable, since photons that travel only a short distance are usually not important for the discharge dynamics.

In this work we consider three possible expansions for the absorption function, which we denote by

B2: Bourdon's two-term expansion

B3: Bourdon's three-term expansion

L: Luque's two-term expansion

Luque's parameters [20] are defined in such a way that the ξ from equation (6) is incorporated in the c_i coefficients from equation (7). Therefore results obtained with these parameters do not precisely correspond to $\xi = 0.075$, which is used for the other photoionization methods. For details about these differences and the parameters that are used in this paper see Appendix A of [23].

3.2. Stochastic (Monte Carlo) approach

Another approach is to use Monte Carlo methods to model photoionization as a stochastic process, which it of course also is in real discharges due to the discreteness of photons. This approach was first described in [22], where it was used for PIC simulations. We use the implementation described in chapter 11 of [33], which was also used in [13]. The same approximations are made as for the continuum approach: photon scattering is neglected and photon directions are isotropic. In the limit of an infinite number of infinitesimal photons, the stochastic photoionization profile therefore agrees with the solution of equation (4). The computation of

stochastic photoionization profile consists of several steps:

- (i) The discrete number of ionizing photons in each cell within a given time step Δt is sampled from a Poisson distribution, with the mean given by eq. (6). For a detailed description, see chapter 11 of [33].
- (ii) For each photon, an absorption length is sampled from eq. (5), and a direction from an isotropic distribution is determined using random numbers. Together, these numbers determine the absorption location of the UV photons.
- (iii) The absorption locations of the photons are mapped to grid densities using bi/trilinear interpolation. For this study, this mapping is always done on the finest available grid.

We make use of photons with a weight $w = 1$, so that each computational photon corresponds to a physical photon. By using *super-photons* for which $w > 1$, the computational cost of the method can be reduced, but unphysical noise is introduced. Conversely, *sub-photons* for which $w < 1$ could also be used to reduce the physical noise in the solution.

Even when using physical photons the noise in our simulations is still somewhat underestimated, since we are using a fluid approximation for electrons and ions. Electrons produced in photoionization events do not move (and ionize neutrals) as discrete particles, but instead they correspond to advecting patches of increasing electron density. Furthermore, when photoionization events occur in regions with a coarse grid, the fine-scale noise in the photoionization profile is not captured.

We remark that it is also possible to sample discrete photons from a photoionization profile computed with a continuum method. However, a pure Monte Carlo approach has several advantages: it does not need to introduce any assumptions about the absorption function, and it can easily be adapted to include surface and object interactions.

4. Results and discussion

4.1. Stochastic vs. continuum photoionization in 3D

In this section we compare 3D simulations with stochastic and continuum photoionization, using the computational domain and the initial conditions described in section 2.2. Figure 2 shows an example of the discharge evolution with stochastic photoionization. Initially, the positively charged seed enhances the background field, and a single positive streamer starts to grow downwards. As the streamer propagates downwards, several small

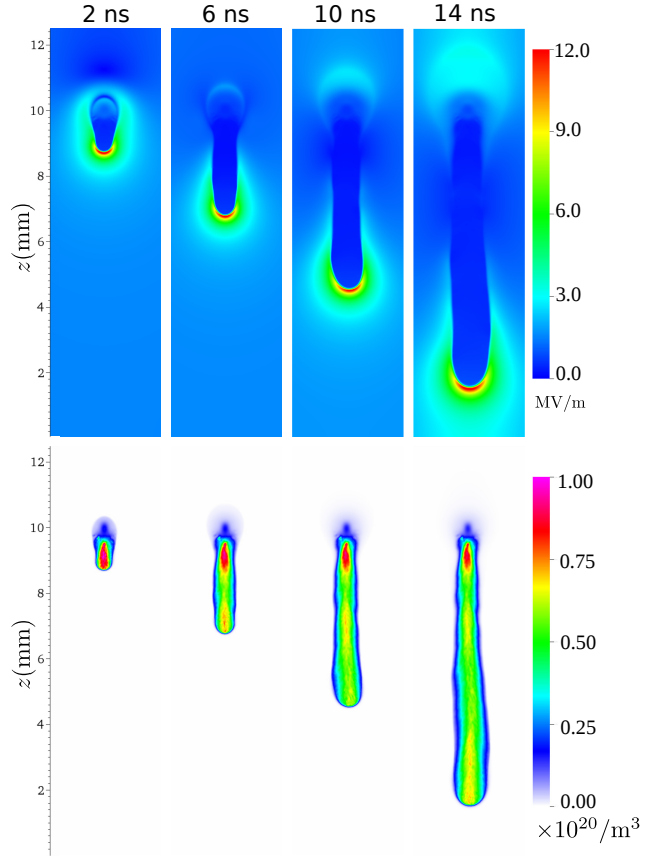


Figure 2: Cross sections in the xz plane showing the evolution of the electric field (top) and the electron density (bottom) in a 3D simulation. Due to stochastic photoionization, fluctuations are visible in the positive streamer's downwards propagation. The width of the domain in the x -direction is 1.25 cm; only a part of it is shown here.

horizontal deviations are visible. After about 16 ns, the streamer reaches the bottom electrode.

To determine the average behavior and the variability of the results with stochastic photoionization, we performed ten runs, each with a different initial state of the random number generator. Figure 3 shows volume renders of the electron density at $t = 13$ ns for these runs. For comparison, results with continuum photoionization are also shown, using Luque's two-term and Bourdon's two- and three-term parameters, see section 3.1. In all cases the streamer bridges the gap without branching, and in terms of propagation length there is quite good agreement between the photoionization methods. With stochastic photoionization, small fluctuations in the electron density and propagation length are visible.

The stochastic fluctuations appear to be more pronounced at the beginning of the streamer channel. The reason is probably that the noise in the photo-

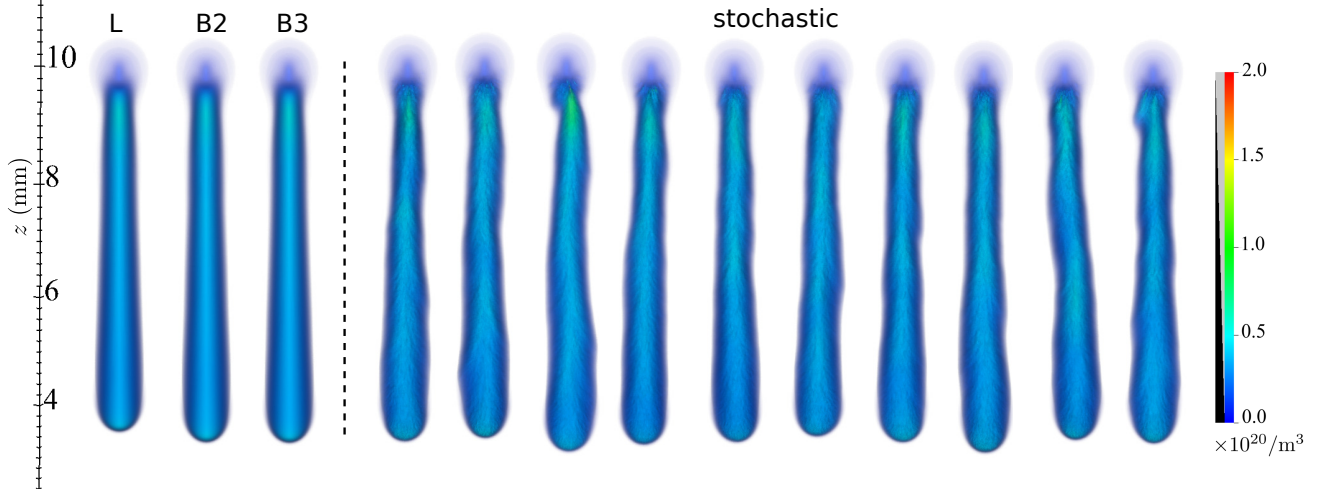


Figure 3: Volume renders of electron density at $t = 13$ ns for the simulations in 3D. Ten stochastic runs, each with a different initial state of the random number generator, are shown on the right. The results with continuum photoionization (with L , B_2 , and B_3 parameters) are shown on the left.

electron density is larger during the start of the streamer. Later on, the region ahead of the streamer has been exposed to photoionization for a longer period, and more photons are produced per unit time. This is illustrated in figure 4, which shows cross sections of the electron density around the streamer head at $t = 1$ ns and $t = 13$ ns on a logarithmic scale. With continuum photoionization, the electron density ahead of the streamer is smooth, whereas clear fluctuations in the electron density are visible with stochastic photoionization, in particular at $t = 1$ ns.

To more quantitatively compare the simulations, the streamer length L , maximal electric field E_{\max} and velocity v are shown in figure 5. The streamer length is defined as $L(t) = L_{\text{domain}} - z_{\max}(t)$, where z_{\max} is the z -coordinate where the electric field is maximal and $L_{\text{domain}} = 1.25$ cm is the domain size. To show variations in length more clearly, figure 5 shows $L(t) - vt$ with $v = 0.05$ cm/ns, and E_{\max} and v are shown as a function of streamer length, to allow for a comparison of streamer properties at the same propagation length. The averages of the ten runs with stochastic photoionization are indicated with error bars. The error bars indicate plus and minus one standard deviation σ of the underlying ten samples, and thus not the standard error of the mean, which would be given by $\sigma/\sqrt{10}$.

For the streamer length, figure 5 shows very good agreement between the averaged stochastic results and the continuum case with Bourdon's parameters (B_2 and B_3). With Luque's photoionization parameters (L) the streamer is a bit slower, but the difference is less than 0.5 mm at any time. This is probably related to the slightly different definition of Luque's parameters,

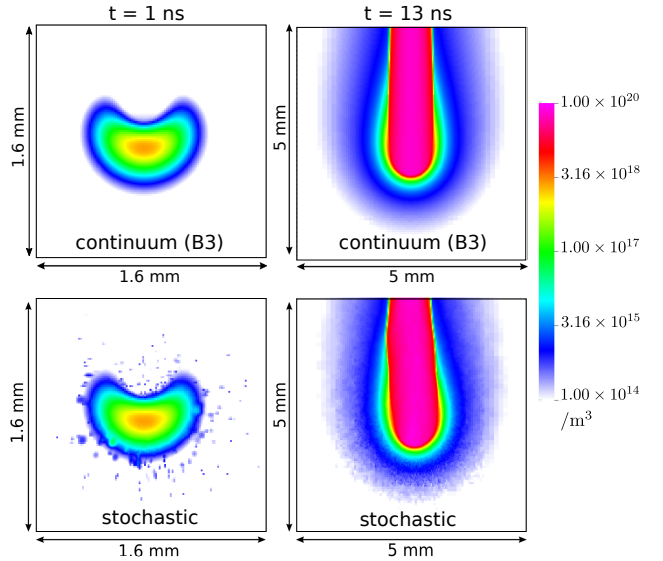


Figure 4: Cross sections of electron density in xz plane around the streamer head for the 3D simulations at $t = 1$ ns and $t = 13$ ns. Top: the results with continuum (B_3 parameters) photoionization. Bottom: the results with stochastic photoionization.

as discussed in section 3.1.

The maximal electric field first increases rapidly, indicating that a streamer has formed, and it then decreases slowly as the streamer propagates across the gap. When the streamer approaches the bottom boundary an increase is again visible, due to the compression of a voltage difference in a small region. The standard deviation of the maximal field is initially around 10 kV/cm in the stochastic runs, but it becomes

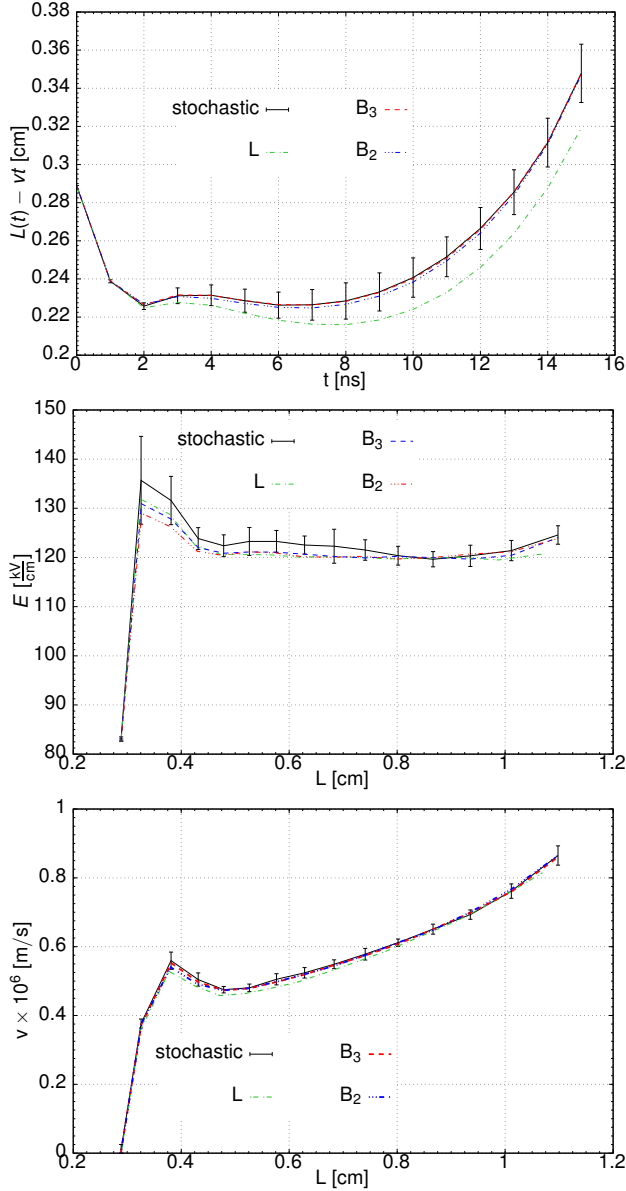


Figure 5: Top: $L(t) - vt$ ($v = 0.05$ cm/ns), where L is the streamer length. Middle: maximal electric field versus streamer length. Bottom: velocity versus streamer length. L , B_2 , and B_3 indicate the results with continuum photoionization. The average results for the ten stochastic runs are indicated with “stochastic”. The error bars indicate plus and minus one standard deviation of the underlying samples.

considerably smaller at later times. This is due to the larger fluctuations in the early stage of the discharge, as also illustrated in figure 4. These fluctuations are probably also the reason why the average maximal field is a bit higher than in the continuum results.

Fluctuations in the streamer velocity are much smaller than in the electric field, and all photoionization approaches show good agreement. Overall, we conclude that under the conditions used in this paper, stochastic photoionization leads to relatively small fluctuations in streamer properties, and that we find good agreement between the average stochastic behavior and the continuum results.

4.2. Comparison with axisymmetric simulations

Single streamers have often been simulated with axisymmetric models [1, 23, 34–37], which are computationally much cheaper than 3D models. When stochastic effects are included, there are a couple of important differences between 3D and axisymmetric models. With axial symmetry, streamers cannot deviate off-axis, unless they branch into an unphysical conical shape [38]. Furthermore, stochastic fluctuations are averaged over the azimuthal direction, which leads to smaller fluctuations at larger radii (because they are averaged over a larger volume).

To investigate how axisymmetric simulations are affected by stochastic photoionization, we repeat the simulations presented in section 4.1 with an axisymmetric model. The same procedure for stochastic photoionization is used as in 3D, but the ionizing photons are now mapped to an (r, z) mesh, where $r^2 = x^2 + y^2$. Another difference is that the cylindrical domain has a radius $R = 1.25$ cm, whereas the 3D simulations were performed in a cube of $(1.25 \text{ cm})^3$. This should only have a small effect, because the streamer is quite far from the lateral boundaries in both cases.

As before, ten runs are performed with different random numbers. Figure 6 shows the electron density at $t = 13$ ns for these ten runs, together with cross sections of the 3D simulations for comparison. In all cases the axisymmetric streamer bridges the gap without branching. Fluctuations in propagation length and in electron density are comparable to those in the 3D simulations. Lateral deviations are of course only visible in the 3D results.

For a more quantitative comparison, figure 7 shows streamer length, maximal electric field and velocity (as in section 4.1). With stochastic photoionization, there is reasonably good agreement between the 3D and axisymmetric results. The error bars indicate plus and minus one standard deviation of the underlying samples, as in section 4.1. Differences up to about one standard deviation are visible in the

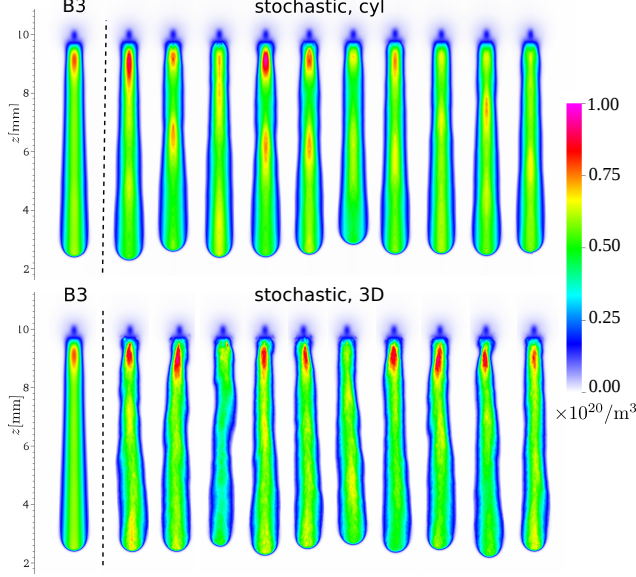


Figure 6: The electron density at $t = 13$ ns for the axisymmetric simulations (top), and the 3D simulations (bottom). Cross sections of the electron density in the xz plane are shown for the 3D simulations. The ten stochastic runs for each case as well as the results with continuum photoionization (B_3) are shown.

maximal electric field, and on average the maximal field is a bit higher in the 3D simulations. This is probably due to small deformations of the streamer's shape that can enhance the field in 3D, see e.g. figure 2.

Results with continuum photoionization are also included in figure 7, using Bourdon's three-term parameters. Without stochastic effects, differences can only arise due to the different numerical discretization of the equations, and due to the slightly different computational domain. The agreement between the 3D and axisymmetric results is excellent, in particular in terms of the maximal field and the streamer's velocity. The agreement is also clear from figure 6, which shows the electron density at $t = 13$ ns for both cases (on the left).

As mentioned above, stochastic noise is smaller at larger radii in axisymmetric simulations, because the grid cells there correspond to larger volumes. This is illustrated in figure 8, which shows the stochastic and continuum production rate of photoelectrons at $t = 13$ ns on a logarithmic scale. Near the axis, the fluctuations are clearly strongest. Note that the continuum and stochastic profile agree reasonably well, at least on a logarithmic scale. We remark that with the stochastic approach the number of ionizing photons produced during a time step depends on the length of

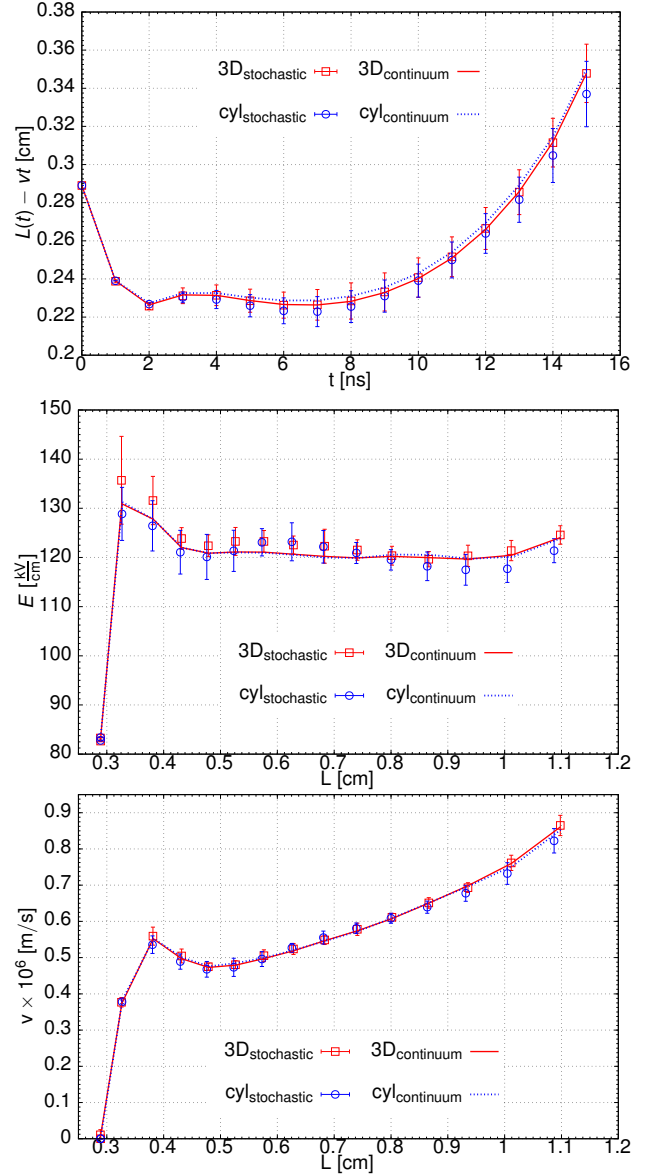


Figure 7: 3D vs. axisymmetric. From top to bottom: $L(t) - vt$ ($v = 0.05$ cm/ns), maximal electric field, velocity. Results with continuum (B_3) and stochastic photoionization are shown. The axisymmetric results are indicated with “cyl”, and 3D results with “3D”.

the time step (see section 3.2), which was here about 2 ps.

In conclusion, stochastic fluctuations also lead to small fluctuations in streamer properties when an axisymmetric model is used. The fluctuations are comparable to the ones observed in 3D, but lateral deviations in the streamer's direction can no longer be modeled. Overall, the results are in good agreement, both between axisymmetric and 3D and between continuum and stochastic photoionization.

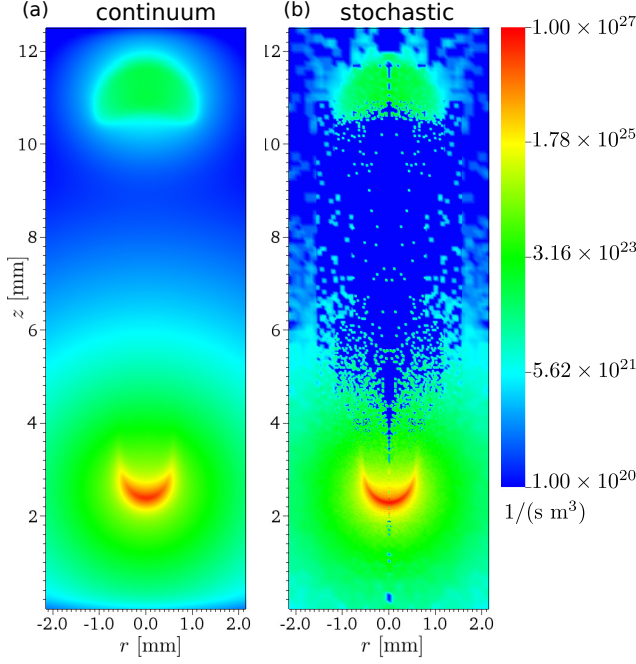


Figure 8: The production rate of photoelectrons (on a logarithmic scale) at $t=13$ ns in an axisymmetric model using (a) continuum photoionization (B_3) and (b) stochastic photoionization.

This agreement will of course only hold as long as the 3D streamers are approximately axisymmetric, which is the case here.

4.3. Changing the amount of photoionization

In this section we investigate how changing the amount of photoionization affects the streamer's propagation. We adjust the amount of photoionization by changing the parameter ξ in equation (6). Other ways to vary the amount of photoionization are changing the gas mixture or the gas pressure, which affects the generation rate as well as the absorption length of the UV photons.

Using the conditions from section 4.1, in which ξ was set to 0.075, we have performed two additional sets of simulations: five runs for $\xi = 0.0375$ and five runs for $\xi = 0.15$. These cases correspond to half and double the amount of photoionization, although only approximately, since the discharge itself will also change with ξ . Figure 9 shows volume renders of the electron density for these simulations at $t = 12$ ns, together with results from section 4.1. For comparison, results with continuum photoionization are also shown in figure 9, using Bourdon's three-term parameters.

Whereas the results with continuum photoionization hardly change, the stochastic simulations are sur-

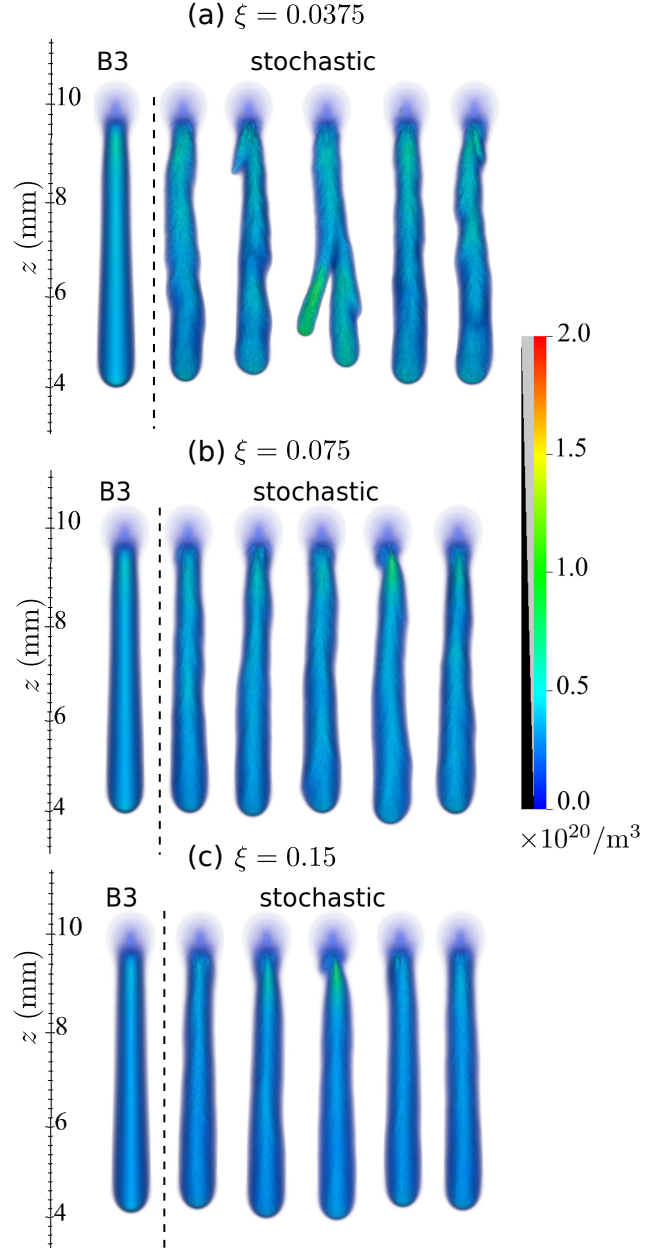


Figure 9: Volume renders of electron density at $t = 12$ ns for 3D simulations with (a) $\xi = 0.0375$, (b) $\xi = 0.075$, (c) $\xi = 0.15$. The parameter ξ controls the amount of photoionization, see equation (6). Five stochastic runs, each with a different initial state of the random number generator are shown on the right. The results with continuum photoionization (B_3) are shown on the left.

prisingly sensitive to the amount of photoionization. For $\xi = 0.0375$, fluctuations in the electron density profile are significantly larger than in the other cases. In one of the five runs, these fluctuations lead to branching, and the branched streamer has the shortest length. For $\xi = 0.075$ and $\xi = 0.15$, the streamers always bridge the gap without branching. The increase in photoionization for $\xi = 0.15$ leads to a smoother electron density profile than for $\xi = 0.075$, but differences in propagation length appear to be similar. Figure 9 also shows that streamer velocities are not sensitive to the amount of photoionization, except for the case with streamer branching, which is in agreement with the results of [39].

In conclusion, the simulations with stochastic photoionization are much more sensitive to the amount of photoionization than those with continuum photoionization. With stochastic photoionization, a decrease in the number of photoelectrons initially leads to more noise, which causes different types of protrusion to form in the streamer channel. If the fluctuations are strong enough, these protrusions can even lead to spontaneous branching. This suggests that stochastic photoionization should be taken into account to model streamer branching, in particular in gas mixtures with less photoionization than air. If we increase the amount of photoelectrons, the streamer channel develops more smoothly than in section 4.1, but there are still small differences in the propagation length.

5. Conclusions

For positive streamer discharges, photoionization is often an important mechanism to provide free electrons ahead of the streamer. Depending on the number of photoionization events and on the volume in which they take place, the photoionization profile can vary from smooth to noisy. In this paper, we have investigated how important such stochastic fluctuations are for positive streamers in atmospheric air. We remark that photoionization is not the only possible source of stochastic fluctuations. Spatial variations in the background ionization density can also affect the propagation and branching of streamers, see e.g. [28]. Conversely, in conditions where a reasonably high background ionization is included, the stochastic effects of photoionization do not play a significant role.

We performed numerical simulations with a 3D plasma fluid model in which photoionization could be included as a stochastic or as a continuum process. Stochastic photoionization profiles were computed with a Monte Carlo method, in which individual ionizing photons were modeled. Continuum photoionization profiles were computed using the Helmholtz approxi-

mation. The evolution of positive streamers between two planar electrodes was simulated, in a background field of 15 kV/cm which is about half of the breakdown field. With stochastic photoionization, we observed fluctuations in streamer properties such as maximal electric field, velocity and electron density. In the test cases considered here, these fluctuations were not strong enough to cause branching. When the stochastic results were averaged, they were in good agreement with the results obtained with continuum photoionization.

Axisymmetric models are commonly used for the simulation of single streamers, because they are computationally much cheaper. However, due to their imposed symmetry, such models cannot properly capture stochastic fluctuations. To see how much this affects simulation results, we compared our 3D simulations to axisymmetric ones. With continuum photoionization, the results agreed very well. With stochastic photoionization, the axisymmetric results showed similar fluctuations in streamer length, maximal electric field and streamer velocity as the 3D simulations. On average, these streamer properties were in good agreement with the 3D simulations.

Finally, we compared stochastic and continuum photoionization for cases with half and double the amount of photoionization. With double the amount of photoionization, stochastic fluctuations were reduced, and there was good agreement between the stochastic and continuum results. With half the amount of photoionization, stochastic fluctuations became much more important, and branching started to occur. Our results are therefore surprisingly sensitive to the amount of photoionization. Because of this sensitivity, we expect that stochastic photoionization can cause streamer branching in other discharge configurations in atmospheric air (i.e., without an artificially reduced photoionization level). For example, the background field used here is homogeneous, whereas the field from a pointed electrode can have strong lateral components that accelerate branching. Furthermore, for discharges developing in lower background fields the stochastic effects of photoionization can be stronger.

In conclusion, we find good agreement between the averaged stochastic simulations and the continuum simulations in our test cases in atmospheric air. However, stochastic fluctuations significantly increase when the amount of photoionization is reduced. In other gas mixtures or different discharge conditions, the stochastic effects of photoionization could therefore play an important role in the propagation and branching of positive streamers.

6. Acknowledgments

B.B. acknowledges funding through the Dutch TTW-project 15052, and J.T. through postdoctoral fellowship 12Q6117N of the Belgian-Flemish FWO. The authors gratefully acknowledge Ute Ebert for her profound comments and discussions during this work.

The simulation code used in this paper is available at <https://gitlab.com/MD-CWI-NL/afivo-streamer>. Moreover the input files for generating the results together with the output files are provided in <https://doi.org/10.17026/dans-zec-672a>.

References

- [1] Vitello P A, Penetrante B M and Bardsley J N 1994 *Physical Review E* **49** 5574–5598 ISSN 1095-3787 URL <http://dx.doi.org/10.1103/PhysRevE.49.5574>
- [2] Yi W J and Williams P F 2002 *J. Phys. D: Appl. Phys.* **35** 205–218 ISSN 1361-6463 URL <http://dx.doi.org/10.1088/0022-3727/35/3/308>
- [3] Ebert U, Nijdam S, Li C, Luque A, Briels T and van Veldhuizen E 2010 *Journal of Geophysical Research* **115** ISSN 0148-0227 URL <http://dx.doi.org/10.1029/2009JA014867>
- [4] Nijdam S, van de Wetering F M J H, Blanc R, van Veldhuizen E M and Ebert U 2010 *J. Phys. D: Appl. Phys.* **43** 145204 ISSN 1361-6463 URL <http://dx.doi.org/10.1088/0022-3727/43/14/145204>
- [5] An W, Baumung K and Bluhm H 2007 *Journal of Applied Physics* **101** 053302 ISSN 1089-7550 URL <http://dx.doi.org/10.1063/1.2437675>
- [6] Sentman D D and Wescott E M 1995 *Phys. Plasmas* **2** 2514 ISSN 1070-664X URL <http://dx.doi.org/10.1063/1.871213>
- [7] Fridman A, Chirokov A and Gutsol A 2005 *Journal of Physics D: Applied Physics* **38** R1R24 ISSN 1361-6463 URL <http://dx.doi.org/10.1088/0022-3727/38/2/R01>
- [8] Adamovich I, Baalrud S D, Bogaerts A, Bruggeman P J, Cappelli M, Colombo V, Czarnetzki U, Ebert U, Eden J G, Favia P and et al 2017 *Journal of Physics D: Applied Physics* **50** 323001 ISSN 1361-6463 URL <http://dx.doi.org/10.1088/1361-6463/aa76f5>
- [9] Kanazawa S, Kawano H, Watanabe S, Furuki T, Akamine S, Ichiki R, Ohkubo T, Kocik M and Mizeraczyk J 2011 *Plasma Sources Science and Technology* **20** 034010 ISSN 1361-6595 URL <http://dx.doi.org/10.1088/0963-0252/20/3/034010>
- [10] Starikovskaia S M 2014 *J. Phys. D: Appl. Phys.* **47** 353001 ISSN 1361-6463 URL <http://dx.doi.org/10.1088/0022-3727/47/35/353001>
- [11] Nozaki T and Okazaki K 2013 *Catalysis Today* **211** 29–38 ISSN 0920-5861 URL <http://dx.doi.org/10.1016/j.cattod.2013.04.002>
- [12] Briels T M P, Kos J, Winands G J J, van Veldhuizen E M and Ebert U 2008 *J. Phys. D: Appl. Phys.* **41** 234004 ISSN 1361-6463 URL <http://dx.doi.org/10.1088/0022-3727/41/23/234004>
- [13] Nijdam S, Teunissen J, Takahashi E and Ebert U 2016 *Plasma Sources Science and Technology* **25** 044001 ISSN 1361-6595 URL <http://dx.doi.org/10.1088/0963-0252/25/4/044001>
- [14] Pancheshnyi S 2005 *Plasma Sources Sci. Technol.* **14** 645–653 ISSN 1361-6595 URL <http://dx.doi.org/10.1088/0963-0252/14/4/002>
- [15] Zheleznyak M B, Mnatsakanian A K and Sizykh S V 1982 *Teplofizika Vysokikh Temperatur* **20** 423–428
- [16] Pancheshnyi S 2014 *Plasma Sources Sci. Technol.* **24** 015023 ISSN 1361-6595 URL <http://dx.doi.org/10.1088/0963-0252/24/1/015023>
- [17] Stephens J, Fierro A, Beeson S, Laity G, Trienekens D, Joshi R P, Dickens J and Neuber A 2016 *Plasma Sources Science and Technology* **25** 025024 ISSN 1361-6595 URL <http://dx.doi.org/10.1088/0963-0252/25/2/025024>
- [18] Stephens J, Abide M, Fierro A and Neuber A 2018 *Plasma Sources Science and Technology* **27** 075007 ISSN 1361-6595 URL <http://dx.doi.org/10.1088/1361-6595/aacc91>
- [19] Jiang M, Li Y, Wang H, Zhong P and Liu C 2018 *Physics of Plasmas* **25** 012127 ISSN 1089-7674 URL <http://dx.doi.org/10.1063/1.5019478>
- [20] Luque A, Ebert U, Montijn C and Hundsdoerfer W 2007 *Appl. Phys. Lett.* **90** 081501 ISSN 0003-6951 URL <http://dx.doi.org/10.1063/1.2435934>
- [21] Bourdon A, Pasko V P, Liu N Y, Clestin S, Sgur P and Marode E 2007 *Plasma Sources Sci. Technol.* **16** 656–678 ISSN 1361-6595 URL <http://dx.doi.org/10.1088/0963-0252/16/3/026>
- [22] Chanrion O and Neubert T 2008 *Journal of Computational Physics* **227** 7222–7245 ISSN 0021-9991 URL <http://dx.doi.org/10.1016/j.jcp.2008.04.016>
- [23] Bagheri B, Teunissen J, Ebert U, Becker M M, Chen S, Ducasse O, Eichwald O, Loffhagen D, Luque A, Mihailova D, Plewa J M, van Dijk J and Yousfi M 2018 *Submitted to Plasma Sources Sci. Technol.*
- [24] Xiong Z and Kushner M J 2014 *Plasma Sources Science and Technology* **23** 065041 ISSN 1361-6595 URL <http://dx.doi.org/10.1088/0963-0252/23/6/065041>
- [25] Luque A and Ebert U 2011 *Physical Review E* **84** ISSN 1550-2376 URL <http://dx.doi.org/10.1103/PhysRevE.84.046411>
- [26] Li C, Teunissen J, Nool M, Hundsdoerfer W and Ebert U 2012 *Plasma Sources Science and Technology* **21** 055019 ISSN 1361-6595 URL <http://dx.doi.org/10.1088/0963-0252/21/5/055019>
- [27] Teunissen J and Ebert U 2016 *Plasma Sources Science and Technology* **25** 044005 ISSN 1361-6595 URL <http://dx.doi.org/10.1088/0963-0252/25/4/044005>
- [28] Teunissen J and Ebert U 2017 *Journal of Physics D: Applied Physics* **50** 474001 ISSN 1361-6463 URL <http://dx.doi.org/10.1088/1361-6463/aa8faf>
- [29] Dutton J 1975 *Journal of Physical and Chemical Reference Data* **4** 577–856 URL <http://dx.doi.org/doi/10.1063/1.555525>
- [30] Hartmann G 1984 *IEEE Transactions on Industry Applications* **IA-20** 1647–1651 ISSN 0093-9994, 1939-9367 URL <http://ieeexplore.ieee.org/document/4504655/>
- [31] Hagelaar G J M and Pitchford L C 2005 *Plasma Sources Science and Technology* **14** 722–733 ISSN 1361-6595 URL <http://dx.doi.org/10.1088/0963-0252/14/4/011>
- [32] Teunissen J and Ebert U 2018 *Computer Physics Communications* **233** 156166 ISSN 0010-4655 URL <http://dx.doi.org/10.1016/j.cpc.2018.06.018>
- [33] Teunissen J 2015 *3D Simulations and Analysis of Pulsed Discharges* PhD Thesis Technische Universiteit Eindhoven, <http://repository.tue.nl/801516>
- [34] Luque A, Ratushnaya V and Ebert U 2008 *J. Phys. D: Appl. Phys.* **41** 234005 ISSN 1361-6463 URL <http://dx.doi.org/10.1088/0022-3727/41/23/234005>
- [35] Aleksandrov N L and Bazelyan E M 1996 *J. Phys. D: Appl. Phys.* **29** 740–752 ISSN 1361-6463 URL <http://dx.doi.org/10.1088/0022-3727/29/3/035>
- [36] Dhali S K and Williams P F 1987 *Journal of Applied Physics* **62** 4696–4707 ISSN 1089-7550 URL <http://dx.doi.org/10.1063/1.339020>

- [37] Bourdon A, Bonaventura Z and Celestin S 2010 *Plasma Sources Sci. Technol.* **19** 034012 ISSN 1361-6595 URL <http://dx.doi.org/10.1088/0963-0252/19/3/034012>
- [38] Luque A and Ebert U 2012 *Journal of Computational Physics* **231** 904–918 ISSN 0021-9991 URL <http://dx.doi.org/10.1016/j.jcp.2011.04.019>
- [39] Wormeester G, Pancheshnyi S, Luque A, Nijdam S and Ebert U 2010 *J. Phys. D: Appl. Phys.* **43** 505201 ISSN 1361-6463 URL <http://dx.doi.org/10.1088/0022-3727/43/50/505201>